


Crystal-Structure Matches in Solid-Solid Phase Transitions

Fang-Cheng Wang¹, Qi-Jun Ye^{1,2,*}, Yu-Cheng Zhu¹, and Xin-Zheng Li^{1,2,3,†}

¹State Key Laboratory for Artificial Microstructure and Mesoscopic Physics, Frontier Science Center for Nano-optoelectronics, School of Physics, Peking University, Beijing 100871, People's Republic of China

²Interdisciplinary Institute of Light-Element Quantum Materials, Research Center for Light-Element Advanced Materials, and Collaborative Innovation Center of Quantum Matter, Peking University, Beijing 100871, People's Republic of China

³Peking University Yangtze Delta Institute of Optoelectronics, Nantong, Jiangsu 226010, People's Republic of China

 (Received 9 May 2023; revised 1 December 2023; accepted 9 January 2024; published 20 February 2024)

The exploration of solid-solid phase transition suffers from the uncertainty of how atoms in two crystal structures match. We devised a theoretical framework to describe and classify crystal-structure matches (CSM). Such description fully exploits the translational and rotational symmetries and is independent of the choice of supercells. This is enabled by the use of the Hermite normal form, an analog of reduced echelon form for integer matrices. With its help, exhausting all CSMs is made possible, which goes beyond the conventional optimization schemes. In an example study of the martensitic transformation of steel, our enumeration algorithm finds many candidate CSMs with lower strains than known mechanisms. Two long-sought CSMs accounting for the most commonly observed Kurdjumov-Sachs orientation relationship and the Nishiyama-Wassermann orientation relationship are unveiled. Given the comprehensiveness and efficiency, our enumeration scheme provide a promising strategy for solid-solid phase transition mechanism research.

DOI: [10.1103/PhysRevLett.132.086101](https://doi.org/10.1103/PhysRevLett.132.086101)

Solid-solid phase transition (SSPT) is ubiquitous in nature and relevant to many industries [1]. For example, the martensitic transition is a process of immense importance in the steel industry [2–4], and the graphite-to-diamond transition under shock compression enables the synthesis of highly desirable diamond from abundant and cheap carbon sources [5–8]. Compared to other well-studied dynamical processes, such as the gas-phase or surface reactions [9–12], SSPTs involve not only much greater degrees of freedom (d.o.f.) [13–15] but also complex collective behavior with controversial mechanisms [16]. Besides, the crystalline nature highlights the significance of lattice deformation in the reaction path, which is distinct from the fluid-solid or fluid-fluid phase transitions [17,18]. With potential insights into the mechanisms and principles of self-organization, symmetry breaking, and criticality in multiple disciplines, understanding the atomic details of SSPTs is urgent but remains in its infancy.

Theoretical studies of SSPTs fall into two categories: nucleation and concerted mechanisms. Although a realistic SSPT generally occurs through nucleation, the vast d.o.f. it involves are expensive for atomic-level simulations. The concerted mechanism is a simplified model with few d.o.f. in a small supercell with periodic boundary condition, and thus can be investigated at the density-functional theory level [17]. Despite their differences, simulations using $\sim 10^5$ atoms suggest that minimum energy paths (MEP) of nucleation proceed locally via much simpler concerted

mechanisms [13,14]. That is to say, nucleation is likely to share the same atom-to-atom correspondence between the initial and final structures—which we call the crystal-structure match (CSM)—with a concerted mechanism [see Fig. 1(a)]. As a universal concept, the CSM lies at the heart of the SSPT research. This is especially true for concerted mechanisms, where methods to find the MEP like the solid-solid nudged elastic band (SSNEB) require the user to prespecify a pair of supercells in two phases and the correspondence between the atoms in them [17,19]. However, human intuition often fails to select the “best” CSM, in which case the obtained MEP is not the global one. To address this issue, methods like the stochastic surface walking [20] and PALLAS [21] try different CSMs as they explore the potential energy surface. Meanwhile, several studies have been dedicated to design criteria for instructing CSM without explicit energy minimization, e.g., maximal symmetry [22], minimal strain [23], minimal dissociation of chemical bonds [24], and minimal total distance traveled by the atoms [25]. Nevertheless, existing optimization algorithms cannot claim conclusively to find the best CSMs under these criteria, nor are they guaranteed to be energetically favorable.

In this Letter, we provide a theoretical framework to describe, classify, and enumerate CSMs. We call the lattice deformation of a CSM its sublattice match (SLM), since it deforms certain sublattices of the initial crystal structure into sublattices of the final one [see Fig. 1(b)]. By extracting key features of a sublattice as a Hermite normal

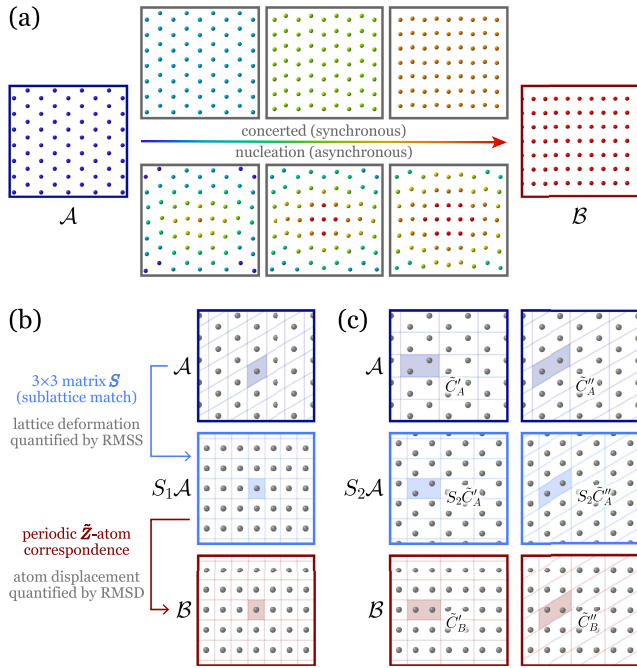


FIG. 1. CSMs between \mathcal{A} (hexagonal) and \mathcal{B} (orthogonal). (a) The same CSM can be established either by concerted mechanisms or by nucleation, where the atoms migrate to their counterparts synchronously or asynchronously. The colors of the atoms represent their own degrees of migration. (b) A CSM consists of an SLM which matches the sublattice of \mathcal{A} to that of \mathcal{B} , and a periodic \tilde{Z} -atom correspondence. In this example we have $\tilde{Z} = 1$. (c) Another CSM with $\tilde{Z} = 2$, whose RMSS is lower but RMSD is higher than (b). The two columns show different supercell pair choices, respectively.

form (HNF) [26,27], we show that every SLM can be uniquely represented by an integer-matrix triplet (IMT). This eliminates the heavy redundancy in the conventional supercell pair representation [17,23,35], making it possible to *exhaust* all SLMs within a certain range. For each SLM, its representative CSM is obtained via the Hungarian algorithm which minimizes the atomic displacement [36]. Using this strategy, we provide a comprehensive list of CSMs in an example study of the martensitic transformation of steel. Among the enumerated CSMs, we discover the ones that account for the most commonly observed Kurdjumov-Sachs (KS) orientation relationship (OR) [37] and the Nishiyama-Wassermann (NW) OR [3], as well as ones with much lower strains than all previously known mechanisms.

Practically, we consider a CSM with the following property [38]: there exists a linear transformation S such that after its deformation, the atoms in the deformed structure $S\mathcal{A}$ correspond to the atoms in \mathcal{B} *periodically*, as shown in Figs. 1(b) and 1(c). Denote the number of atoms in the smallest spatial period by \tilde{Z} . As S transforms the sublattices in \mathcal{A} into those in \mathcal{B} , there exist pairs of \tilde{Z} -atom supercells such that

$$S\tilde{C}_A = \tilde{C}_B, \quad (1)$$

where \tilde{C}_α ($\alpha = A$ or B) is a 3×3 matrix whose columns are supercell vectors arranged in right-handed order. We call S —with the sublattices before and after deformation—the sublattice match (SLM) of this CSM.

Denoting a primitive cell in α by C_α , the supercell is associated with an integer matrix M_α as $\tilde{C}_\alpha = C_\alpha M_\alpha$ [39] with the constraint

$$Z_\alpha \det M_\alpha = \tilde{Z}, \quad (2)$$

where Z_α is the number of atoms in C_α . This means that each (M_A, M_B) satisfying Eq. (2) gives an SLM, as

$$S = C_B M_B M_A^{-1} C_A^{-1}, \quad (3)$$

which we call the supercell pair representation [17,23,35]. However, such supercell pair of a given SLM is not unique [see Fig. 1(c)]. This is because for any integer matrix Q with $\det Q = 1$, another $(M'_A, M'_B) = (M_A Q, M_B Q)$ also gives the same S and satisfies Eq. (2). This redundancy has made the enumeration of SLMs extremely difficult, as reported in Ref. [35].

We overcome this difficulty by utilizing the theorem: any integer matrix M with $\det M > 0$ can be *uniquely* decomposed into two integer matrices as $M = HQ$, where H is in Hermite normal form (HNF) and $\det Q = 1$ [26]. That is to say, under elementary column operations over integers [27], M can be uniquely transformed into

$$H = \begin{bmatrix} h_{11} & 0 & 0 \\ h_{21} & h_{22} & 0 \\ h_{31} & h_{32} & h_{33} \end{bmatrix}, \quad 0 \leq h_{ij} < h_{ii} \quad (j < i), \quad (4)$$

which is an analog of reduced echelon form for integer matrices. Similar techniques have been used in the Hart-Forcade theory, a well-developed framework for generating derivative structures [40–42]. Applying $M_\alpha = H_\alpha Q_\alpha$ to Eq. (3), we obtain

$$S = C_B H_B Q H_A^{-1} C_A^{-1}, \quad (5)$$

where $Q = Q_B Q_A^{-1}$ is an integer matrix with $\det Q = 1$ and H_α is in HNF satisfying

$$\det H_\alpha = \frac{\tilde{Z}}{Z_\alpha}, \quad (6)$$

which is derived from Eq. (2). This IMT representation (H_A, H_B, Q) of a given SLM is *unique*, with which one can prove that the total number of \tilde{Z} -atom SLMs is finite and thus exhaustible as long as the strain is bounded. For mathematical details, see our Supplemental Material [27].

To quantify the strain, we use the quadratic average of the principal strains (PS) of S , which we call the root-mean-square strain (RMSS), but one could well use other criteria.

Given an SLM, the only unspecified part of a CSM is how the \tilde{Z} atoms in \tilde{C}_A are mapped to atoms in \mathcal{B} [43]. Note that the sublattice given by the SLM divides atoms in \mathcal{B} into \tilde{Z} translational equivalence classes. There are at most \tilde{Z} possible ways for a CSM to assign \tilde{Z} atoms in \tilde{C}_A to the \tilde{Z} equivalence classes in \mathcal{B} . When it is unfeasible to check numerous correspondences one by one, there is often a focus on the best one under certain geometric criterion, e.g., the root-mean-square displacement (RMSD) from the atoms in S_A to their counterparts in \mathcal{B} [27]. We call such best CSM the representative of its SLM, which can always be solved via the Hungarian algorithm in polynomial time [36]. We use the RMSS and RMSD to characterize CSMs because they are proportional to the Euclidean distance between structures contributed by the lattice d.o.f. and atomic d.o.f., respectively [27].

In an example study of the martensitic transformation of steel, an SSPT from the austenite phase (fcc, $a_{\text{fcc}} = 3.57 \text{ \AA}$) to the martensite phase (bcc, $a_{\text{bcc}} = 2.87 \text{ \AA}$), we exhaust all SLMs with $\tilde{Z} \leq 36$ and $\text{RMSS} \leq 16\%$ [27]. With 54 178 SLMs enumerated, we compute the representative CSM for each SLM, as shown in Fig. 2. The exhaustion of SLMs is accomplished through the IMT representation: (i) Randomly generate a trial linear transformation S_0 with $\text{RMSS} \leq 16\%$. (ii) Exhaust all H_α 's satisfying Eqs. (4) and (6). For each (H_A, H_B) , compute the nearest integer matrix to the solution of Eq. (5), namely

$$Q_0 = \text{rint}(H_B^{-1} C_B^{-1} S_0 C_A H_A), \quad (7)$$

where ‘‘rint’’ rounds each matrix element to its nearest integer. If $\det Q_0 = 1$ holds, an SLM represented by

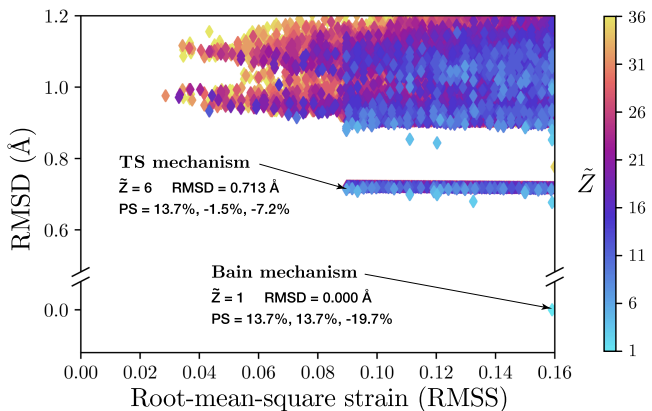


FIG. 2. CSMs of the martensitic transformation of steel. For simplicity, only the representative CSM of each SLM is shown. Arrows point out the Bain mechanism [45] and the Therrien-Stevanović one [4]. Besides them, the vast remaining CSMs have not been reported previously, which might imply new mechanisms.

(H_A, H_B, Q_0) is obtained. (iii) Repeat this process until the number of consecutive replications of SLMs reaches the convergence criterion. The implementation is available as a Python package CRYSTMATCH [44].

To reveal the realistic CSMs, we compare these enumeration results to experiments via orientation relationship (OR) analysis. The OR specifies how the crystallographic axes of the product phase are oriented relative to the parent phase. For experiments on the martensitic transformation of steel, the KS OR and/or NW OR are dominant in bulks [2,3,37], while the Pitsch OR is only reported in thin films [4,46]. These ORs are denoted by parallelisms, as detailed in Ref. [47]. On the other hand, each CSM *a priori* determines an OR through certain regulations. Two most popular and reasonable manners are (i) keeping rotation-free and deforming \mathcal{A} by $\sqrt{S^T S}$, which minimizes the total atomic displacement [27], as used in Ref. [4]; (ii) imposing a rotation to restore the uniformly scaled plane (USP), as suggested by the phenomenological theory of martensitic transformation [48]. We shall show results under both manners.

We benchmarked all CSMs by the KS, NW, and Pitsch ORs, respectively. Their distinctions from each OR are quantified by extra rotation angles, which are alone determined by their SLMs [4,27]. Therefore, we only discuss the representative CSM of each SLM for simplicity. When using the rotation-free manner, there is only one CSM that precisely conforms to each OR, as shown in Figs. 3 and S4 [27]. The CSM reproducing the Pitsch OR is consistent with the Therrien-Stevanović (TS)

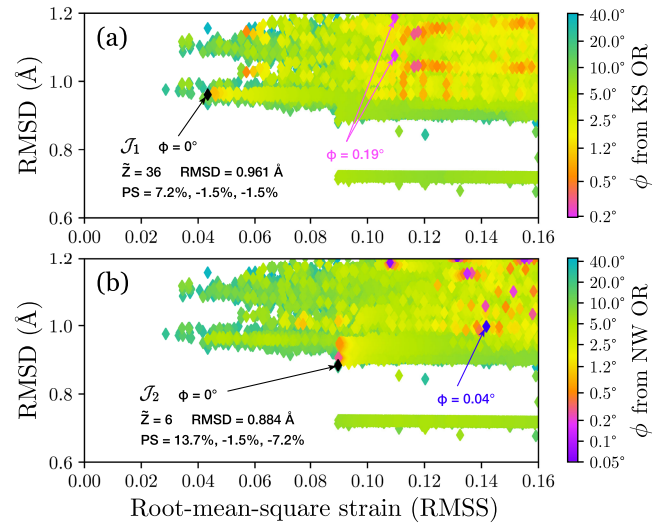


FIG. 3. CSMs benchmarked by the (a) KS and (b) NW ORs. The distinction from an OR is measured by ϕ , the least rotation angle required to produce that OR, as plotted with color bars. For either OR, we find only *one* SLM with exact $\phi = 0$, whose representative CSM is plotted in black as \mathcal{J}_1 and \mathcal{J}_2 . Arrows point out all CSMs with ϕ 's beyond the color bar. For reference, the average deviation of present OR measurements is 0.15° [50].

TABLE I. The main features of the highlighted CSMs.

CSM	\tilde{Z}	RMSS	RMSD (Å)	OR ^a	OR ^b
Bain	1	15.9%	0	Unreported	Unreported
TS	6	9.0%	0.713	Pitsch	KS
\mathcal{J}_1	36	4.3%	0.961	KS	KS
\mathcal{J}_2	6	9.0%	0.884	NW	KS

^aUsing the rotation-free manner.

^bUsing the USP-restoring manner.

mechanism [4], which validates our methods. Besides, we found two new CSMs that reproduce the KS and NW ORs, which are denoted by \mathcal{J}_1 and \mathcal{J}_2 and will be discussed later. When using another manner to restore the USP, we found that 55 CSMs can reproduce the KS OR, including \mathcal{J}_1 , \mathcal{J}_2 , and the TS mechanism (see Fig. S5 [27]), but no enumerated CSM can reproduce the NW or Pitsch OR. The well-studied Bain mechanism [45], which has been proved to have the lowest RMSS among all $\tilde{Z} = 1$ CSMs [49], does not reproduce any observed OR in either manner. Table I highlights the features of these CSMs, where the RMSS and RMSD are calculated from experimental lattice constants. We note that the CSMs accounting for reported ORs have neither the lowest RMSS nor the lowest RMSD among all CSMs (see Figs. 2 and 3). They are thus beyond

the reach of conventional optimization schemes, which further demonstrates the necessity of enumeration.

To gain insight into the mechanisms therein, we illustrate the concerted paths interpolated, respectively, from \mathcal{J}_1 and from \mathcal{J}_2 in Fig. 4. Both paths involve slipping processes along the $(111)_{\text{fcc}} \parallel (011)_{\text{bcc}}$ plane, which occur at every sixth layer and every third layer, respectively. The \mathcal{J}_1 path has an additional intralayer slipping along the $[01\bar{1}]_{\text{fcc}} \parallel [1\bar{1}1]_{\text{bcc}}$ direction. The USPs of both \mathcal{J}_1 and \mathcal{J}_2 coincide with the experimentally observed $\{112\}_{\text{fcc}}$ habit plane [3,51]. Surprisingly, the USP in Fig. 4(a) stays *without* rotation, and even becomes a strictly invariant plane if close-packing lattice constants ($a_{\text{bcc}} = \sqrt{2/3}a_{\text{fcc}}$) are used, which can explain the predominance of the KS OR. Animations of both paths are provided in Supplemental Material [27], where we also apply our scheme to the wurtzite–zinc blende (B4-B3) transition in ZnS, a prototype SSPT involving multiple types of atoms.

Compared to yielding a single optimal CSM by conventional methods, an entire enumeration including the same CSM even takes less time in most cases. Specifically, it takes only 29.17 *seconds* on a single core (3.60 GHz) of Intel Core i7-12700K Desktop Processor to produce all CSMs with $\tilde{Z} \leq 6$ in Fig. 2, which covers all previously reported CSMs. We note that underlying this efficiency is the utilization of symmetries. The translational symmetry is

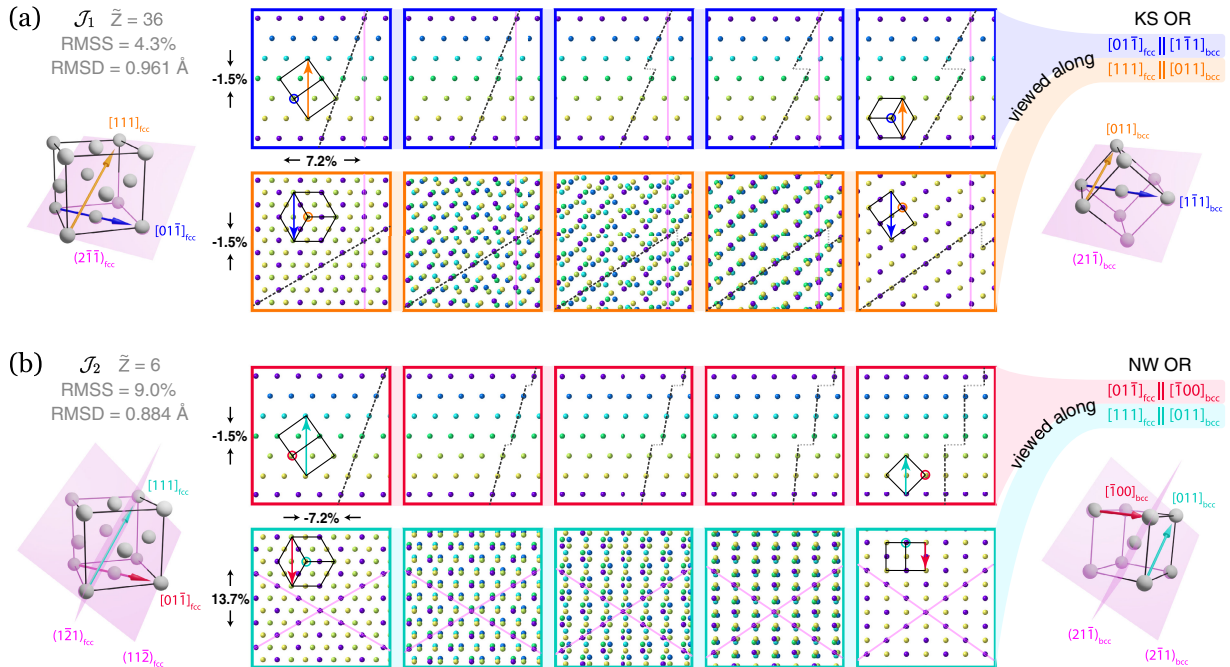


FIG. 4. Concerted paths interpolated, respectively, from \mathcal{J}_1 and from \mathcal{J}_2 . The lattice deformation is assumed to be rotation-free as $\sqrt{S^T S}$, whose principal strains are labeled on the left side of the boxes. The colors of the atoms are used to distinguish different $(111)_{\text{fcc}}$ layers, and dashed lines are used to track the slipping process. Conventional cells of fcc and bcc are edged by solid black lines. USPs are denoted as pink planes. (a) \mathcal{J}_1 accounting for the KS OR, i.e., the parallelism $(111)[01\bar{1}]_{\text{fcc}} \parallel (011)[1\bar{1}1]_{\text{bcc}}$. (b) \mathcal{J}_2 accounting for the NW OR, i.e., the parallelism $(111)[01\bar{1}]_{\text{fcc}} \parallel (011)[\bar{1}00]_{\text{bcc}}$.

implied in the definition of SLM, where a sublattice is a subgroup of the translation group. The exploitation of this crystalline feature frees us from the inherent difficulties in optimizing the rotation, deformation, translation, and atomic correspondence simultaneously, and allows us to deal with 3×3 matrices rather than manipulating large structures with many atoms. By virtue of the rotational symmetry, whenever we obtain a single S , all SLMs of the form $R_B S R_A^{-1}$ are known, where R_α is an element of G_α^{rot} , the group consisting of all rotations that have appeared in the space group of α [27]. This accelerates the enumeration by up to $|G_A^{\text{rot}}| \times |G_B^{\text{rot}}|$ times (e.g., 576-fold faster when exploring the martensitic transformation of steel which have $|G_A^{\text{rot}}| = |G_B^{\text{rot}}| = 24$) and simplifies the results.

The enumerated CSMs can be directly used to study concerted MEPs. With certain geometric criteria [22–25], one can screen out better candidates from enumerated CSMs. This systematically improves the CSM specification in methods like SSNEB. On the other hand, metadynamics simulations have found several nucleation MEPs, which proceed locally through CSMs with small \tilde{Z} 's [14,52,53]. Our scheme can provide a comprehensive list of CSMs covering this range, not only reproducing nucleation-favored CSMs, but also revealing their distinctiveness among all candidates. Additionally, a high-throughput computation [54–56]—the paradigm on the tide—for SSPTs is also enabled, as we presented a framework to describe, classify and enumerate all CSMs. The numerous candidates might contain currently unknown yet realistic mechanisms, which can shed light on the design of more predictive screening criteria, and inspire novel understandings of SSPTs both in nature and in industries.

We acknowledge helpful discussions with J. X. Zeng, H. Y. Yang, R. C. He, J. C. Gao, and W. J. Han. We are grateful to F. Therrien and Z. P. Liu for helpful comments. We are supported by the National Science Foundation of China under Grants No. 12234001, No. 11934003, No. 12204015, and No. 62321004, the National Basic Research Program of China under Grants No. 2021YFA1400503 and No. 2022YFA1403500, the Beijing Natural Science Foundation under Grant No. Z200004, and the Strategic Priority Research Program of the Chinese Academy of Sciences Grant No. XDB33010400. The computational resources were provided by the supercomputer center at Peking University, China.

*qjye@pku.edu.cn

†xzli@pku.edu.cn

- [1] W. D. Callister and D. G. Rethwisch, *Fundamentals of Materials Science and Engineering* (Wiley, London, 2000).
 [2] A. B. Greninger and A. R. Troiano, *JOM* **1**, 590 (1949).

- [3] Z. Nishiyama, *Martensitic Transformation* (Elsevier, New York, 2012).
 [4] F. Therrien and V. Stevanović, *Phys. Rev. Lett.* **125**, 125502 (2020).
 [5] P. S. DeCarli and J. C. Jamieson, *Science* **133**, 1821 (1961).
 [6] D. Erskine and W. Nellis, *Nature (London)* **349**, 317 (1991).
 [7] S. Scandolo, M. Bernasconi, G. L. Chiarotti, P. Focher, and E. Tosatti, *Phys. Rev. Lett.* **74**, 4015 (1995).
 [8] C. J. Mundy, A. Curioni, N. Goldman, I.-F. Will Kuo, E. J. Reed, L. E. Fried, and M. Ianuzzi, *J. Chem. Phys.* **128**, 184701 (2008).
 [9] H. Eyring, *J. Chem. Phys.* **3**, 107 (1935).
 [10] H. Jónsson, G. Mills, and K. W. Jacobsen, in *Classical and Quantum Dynamics in Condensed Phase Simulations* (World Scientific, Singapore, 1998), pp. 385–404.
 [11] G. Henkelman, B. P. Uberuaga, and H. Jónsson, *J. Chem. Phys.* **113**, 9901 (2000).
 [12] A. Heyden, A. T. Bell, and F. J. Keil, *J. Chem. Phys.* **123**, 224101 (2005).
 [13] R. Z. Khaliullin, H. Eshet, T. D. Kühne, J. Behler, and M. Parrinello, *Nat. Mater.* **10**, 693 (2011).
 [14] M. Badin and R. Martoňák, *Phys. Rev. Lett.* **127**, 105701 (2021).
 [15] P. A. Santos-Florez, H. Yanxon, B. Kang, Y. Yao, and Q. Zhu, *Phys. Rev. Lett.* **129**, 185701 (2022).
 [16] F. Therrien, E. B. Jones, and V. Stevanović, *Appl. Phys. Rev.* **8**, 031310 (2021).
 [17] D. Sheppard, P. Xiao, W. Chemelewski, D. D. Johnson, and G. Henkelman, *J. Chem. Phys.* **136**, 074103 (2012).
 [18] P. H. Poole, T. Grande, C. A. Angell, and P. F. McMillan, *Science* **275**, 322 (1997).
 [19] X.-J. Zhang and Z.-P. Liu, *J. Chem. Theory Comput.* **11**, 4885 (2015).
 [20] S.-H. Guan, X.-J. Zhang, and Z.-P. Liu, *J. Am. Chem. Soc.* **137**, 8010 (2015).
 [21] L. Zhu, R. E. Cohen, and T. A. Strobel, *J. Phys. Chem. Lett.* **10**, 5019 (2019).
 [22] C. Capillas, J. Perez-Mato, and M. Aroyo, *J. Phys. Condens. Matter* **19**, 275203 (2007).
 [23] X. Chen, Y. Song, N. Tamura, and R. D. James, *J. Mech. Phys. Solids* **93**, 34 (2016).
 [24] V. Stevanović, R. Trottier, C. Musgrave, F. Therrien, A. Holder, and P. Graf, *Phys. Rev. Mater.* **2**, 033802 (2018).
 [25] F. Therrien, P. Graf, and V. Stevanović, *J. Chem. Phys.* **152**, 074106 (2020).
 [26] H. Cohen, *A Course in Computational Algebraic Number Theory* (Springer Science & Business Media, New York, 2013), Vol. 138, p. 66.
 [27] See Supplemental Material at <http://link.aps.org/supplemental/10.1103/PhysRevLett.132.086101> for detailed results and the mathematical formalism, where Refs. [28–34] are also cited.
 [28] R. G. Bartle and D. R. Sherbert, *Introduction to Real Analysis* (John Wiley & Sons, Inc., 2000), p. 78.
 [29] S. Axler, *Linear Algebra Done Right* (Springer Science & Business Media, New York, 1997).
 [30] A. Sadeghi, S. A. Ghasemi, B. Schaefer, S. Mohr, M. A. Lill, and S. Goedecker, *J. Chem. Phys.* **139**, 184118 (2013).

- [31] A. P. Bartók, R. Kondor, and G. Csányi, *Phys. Rev. B* **87**, 184115 (2013).
- [32] G. Ferré, J.-B. Maillat, and G. Stoltz, *J. Chem. Phys.* **143**, 104114 (2015).
- [33] L. Mirsky, *Monatsh. Math.* **79**, 303 (1975).
- [34] M. Carlsson, *Expo. Math.* **39**, 149 (2021).
- [35] Y.-F. Li and Z.-P. Liu, *Phys. Rev. Lett.* **128**, 226102 (2022).
- [36] H. W. Kuhn, *Nav. Res. Logist. Q.* **2**, 83 (1955).
- [37] G. Kurdjumow and G. Sachs, *Z. Phys.* **64**, 325 (1930).
- [38] Otherwise, the CSM must be described in an infinitely large supercell, which has $\tilde{Z} = \infty$ and is out of the reach of simulations using finitely many atoms. Concerted mechanisms always have finite \tilde{Z} 's, while $\tilde{Z} \leq 12$ generally holds within simulated critical nuclei [13–15].
- [39] A supercell vector is always an integer linear combination of primitive-cell vectors, as $\tilde{\mathbf{v}}_i = \sum_{j=1}^3 m_{ji} \mathbf{v}_j$, where $m_{ij} \in \mathbb{Z}$ are elements of M_α . These vectors form the columns of \tilde{C}_α and C_α in right-handed order, making the determinants of \tilde{C}_α , C_α , and M_α positive.
- [40] A. Santoro and A. D. Mighell, *Acta Crystallogr. Sect. A* **29**, 169 (1973).
- [41] A. Santoro and A. D. Mighell, *Acta Crystallogr. Sect. A* **28**, 284 (1972).
- [42] G. L. W. Hart and R. W. Forcade, *Phys. Rev. B* **77**, 224115 (2008).
- [43] Regardless of the choice of supercell, specifying the counterparts of \tilde{Z} inequivalent atoms always determines a CSM. Therefore, for a given SLM (H_A, H_B, Q) , one may simply let $\tilde{C}_A = C_A H_A$.
- [44] The source code of CRYSTMATCH is available at <https://www.phy.pku.edu.cn/xzli/RESEARCH.htm>, with which one can directly reproduce all results presented in this Letter.
- [45] E. C. Bain and N. Dunkirk, *Trans. AIME* **70**, 25 (1924).
- [46] W. Pitsch, *Philos. Mag.* **4**, 577 (1959).
- [47] K. Koumatos and A. Muehlemann, *Acta Crystallogr. Sect. A* **73**, 115 (2017).
- [48] A. G. Khachaturyan, *Theory of Structural Transformations in Solids* (Courier Corporation, New York, 2013).
- [49] K. Koumatos and A. Muehlemann, *Proc. R. Soc. A* **472**, 20150865 (2016).
- [50] Y. He, S. Godet, and J. J. Jonas, *J. Appl. Crystallogr.* **39**, 72 (2006).
- [51] J. Klostermann and W. Burgers, *Acta Metall.* **12**, 355 (1964).
- [52] A. Laio and M. Parrinello, *Proc. Natl. Acad. Sci. U.S.A.* **99**, 12562 (2002).
- [53] R. Martoňák, A. Laio, and M. Parrinello, *Phys. Rev. Lett.* **90**, 075503 (2003).
- [54] A. Jain, S. P. Ong, G. Hautier, W. Chen, W. D. Richards, S. Dacek, S. Cholia, D. Gunter, D. Skinner, G. Ceder *et al.*, *APL Mater.* **1**, 011002 (2013).
- [55] J. E. Saal, S. Kirklin, M. Aykol, B. Meredig, and C. Wolverton, *JOM* **65**, 1501 (2013).
- [56] S. Curtarolo, W. Setyawan, G. L. Hart, M. Jahnatek, R. V. Chepulskii, R. H. Taylor, S. Wang, J. Xue, K. Yang, O. Levy *et al.*, *Comput. Mater. Sci.* **58**, 218 (2012).